Anisotropic thermal conductivity of high bandwidth memory

Darshan Chalise [1,2], David G. Cahill[1,2,3]*

[1]Department of Physics, University of Illinois at Urbana-Champaign, Urbana, IL, 61801, USA

[2]Materials Research Laboratory, University of Illinois at Urbana-Champaign, Urbana, IL, 61801, USA

[3]Materials Science and Engineering, University of Illinois at Urbana-Champaign, Urbana, IL, 61801, USA

*Corresponding Author – darshan2@illinois.edu

Abstract

Thermal management of integrated circuits (ICs) is important to prevent thermal hotspots which are the leading cause of IC failure. Thermal management is even more critical in 3D integrated circuits (3D ICs) as the prevalence of thermal hotspots is expected to increase due to the presence of polymers and solder materials that are of low thermal conductivity. Understanding how thermal conductivity is affected by the presence of these materials is required for developing thermally aware IC design. The 3ω method can measure thermal conductivities spanning several orders of magnitude and is appropriate for measuring the thermal properties of layered structures such as 3D ICs. In this work, we use the 3ω method with planar and cylindrical heat flow geometries to determine thermal conductivities of the memory layers and layers with polymer and solder bumps in High Bandwidth Memory (HBM) Random Access Memory (RAM). We determine the in-plane thermal conductivity of the memory layers in HBM as 140 ± 13 W/m-K, while the through-plane conductivity of the polymer/solder bump layer is 2 ± 0.2 W/m-K. Combining the results of x-ray tomography and the 3ω measurements, we estimate that the effective in-plane thermal conductivity of the overall HBM device is 100 ± 10 W/m-K while the effective through-plane thermal conductivity is 7 ± 0.7 W/m-K. Our results show that the presence of polymers and solder metals results in a significantly decreased through-plane thermal conductivity of a 3D IC compared to a single IC die. Improvement in the thermal performance of 3D ICs will require improvement in the thermal conductivity or the increased contact area of the solder metals used in 3D ICs.

1.INTRODUCTION

Thermal hotspots are the leading cause of failure of integrated circuits [1], [2]. In 3D integrated circuits (3D ICs), the prevalence of thermal hotspots is expected to increase due to the presence of polymer layers affecting the transfer of heat between dies and from the integrated circuits to the heat spreaders or heat sink [1]. Knowledge of the thermal conductivities in all directions of a 3D IC is important to understand the thermal performance of different components in a 3D IC. Knowing the thermal conductivities in different directions also helps in understanding how stacking affects the thermal performance of ICs and aids in strategic placement of heat spreaders and heat sinks for effective thermal management.

Steady-state thermal conductivity measurement techniques [3], which involve imposing a heat flux and measuring the temperature gradient across the sample, or imposing a temperature gradient and measuring the heat flux, can be used for thermal conductivity measurements. However, steady-state techniques typically require the use of thermal interface grease to improve the thermal contact between a sample and the measurement apparatus. For samples that are thin or have a high thermal conductivity, i.e., the thermal resistance of the sample is not large, the thermal resistance of the grease makes a significant contribution to the overall thermal resistance [4]. Small errors in estimating the thickness of the grease can induce significant errors in estimating the sample thermal conductivity.

Transient thermal conductivity measurement techniques, for e.g., time domain thermoreflectance (TDTR) [5] or the 3ω method [6] do not require the use of thermal interface materials and can be used for measuring samples with thermal conductivity spanning several orders of magnitude [6], [7]. These techniques can also be used to measure both in-plane and through plane thermal conductivities in samples which have anisotropic thermal conductivity [7]–[9].

An important concept in transient thermal conductivity measurement is the concept of thermal penetration depth δ, which is the distance heat diffuses in a measurement time [7]. In frequency domain, the thermal penetration depth is given by $\delta = \sqrt{\frac{D}{\omega_H}}$ for heating at frequency ω_H [6]. Here, the thermal diffusion constant D is the ratio of thermal conductivity κ and volumetric heat capacity C_v. For a 3ω measurement with an ac excitation frequency ω, the 2ω heating results in a thermal penetration depth $\delta = \sqrt{\frac{D}{2\omega}}$. By varying the frequency of the 3ω measurement, the thermal penetration depth can be changed, and therefore, the thermal properties of different layers in a layered structure can be probed. The thermal penetration depth of the measurement can span from microns to millimeters as the frequency is varied from a few tens of mHz to a few kHz [9]. Our results using x-ray tomography show that the length scale of the heterogeneities in 3D ICs is of the order ~ 100 microns in the through-plane direction (z-direction). Therefore, the 3ω method is an appropriate technique in decoupling the thermal conductivities of different layers in a stacked 3D IC.

In this work, we perform measurements of the thermal conductivities of the memory and polymer layers of a prototypical 3D IC, a High Bandwidth Memory (HBM) Random Access Memory (RAM) [10], using the 3-omega method. We combine measurements of the thermal conductivity of different layers with the results from x-ray tomography to estimate the effective thermal conductivities of the in-plane and through-plane directions. The results of this study elucidate how layering of materials affects the thermal performance of electronic devices and aids the design of thermal management strategies for 3D ICs.

2. DETERMINATION OF HBM STRUCTURE

2.1. Sample preparation

The second generation of high bandwidth memory, High Bandwidth Memory 2 (HBM2) samples were extracted from an off-the-shelf graphic card. Two HBM2 devices were separated from the CPU. The interposer layer containing the CPU and the HBM device was first removed from the substrate by melting the solder joints connecting the interposer and the substrate. The interposer was then cut to isolate the HBMs from the CPU. The remaining interposer was ground until the logic die (bottom die) of the HBM was exposed.

We used a vernier caliper with a precision of 100 μm to measure the dimensions of the sample. The isolated HBM2 samples had dimensions of 6 mm ×10 mm at the top and 7 mm ×11 mm at the bottom. We estimate the top 4 memory layers to be 6 mm ×10 mm and the base die to be 7 mm ×11. The sample had a total thickness of 700 μm.

2.2. X-ray tomography

We used x-ray tomography to obtain a cross sectional image of HBM2. We performed the x-ray tomography with a Rigaku MicroCT system using continuous x-rays from a Mo anode with an acceleration voltage of 47 kV. The imaging was performed on the middle portion of HBM2 with a 6 mm × 4 mm field of view. 1440 x-ray absorption images were collected with a sample rotation of 360°. 1098 images were reconstructed along the cross section of the HBM2 with a pixel size of 1 μm × 1 μm.

We processed the image using Matlab ® and used ImageJ to determine the thickness of each layer.

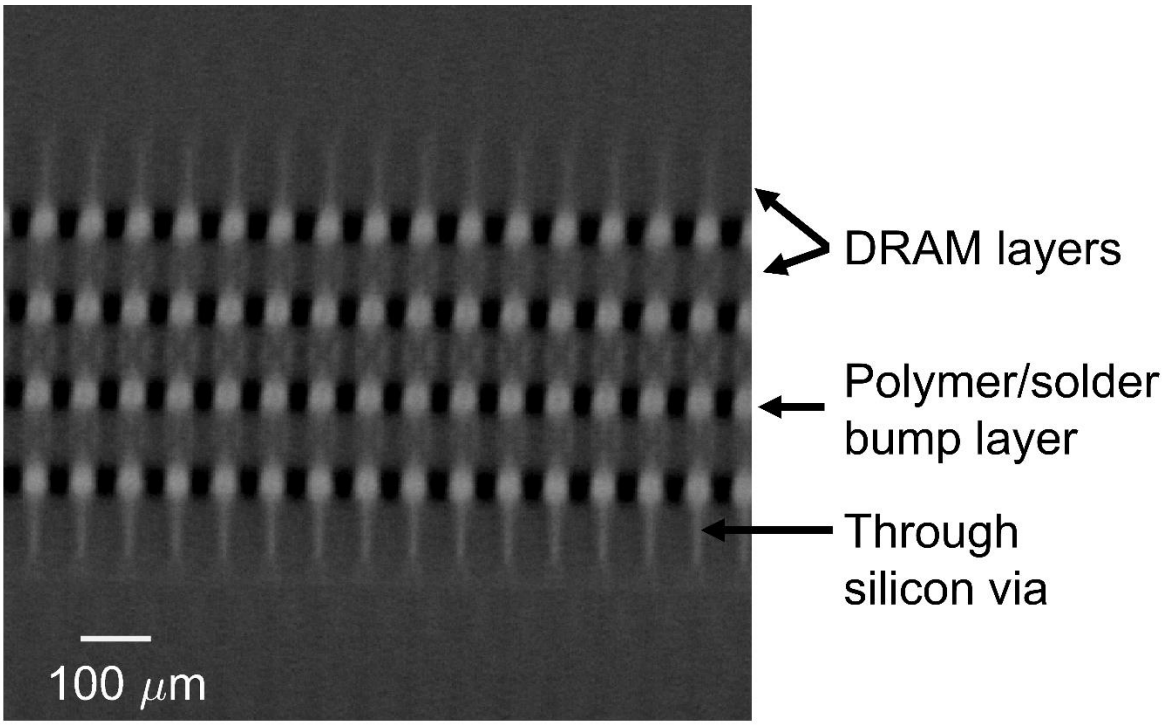

Figure 1. X-ray absorption computed tomography of the cross section of HBM. The displayed image is a 1.2 × 1.1 mm^2 section of a reconstructed image with a field of view of 6 × 4 mm^2 from the middle of the HBM sample. The x-ray tomography measurement was carried out with a spatial resolution of 1 ×1 μm^2. X-ray tomography shows the top DRAM layer to be ~120 μm thick while the other 3 DRAM layers are each ~80 μm thick. The base logic die is ~150 μm thick. The silicon layers show through silicon vias (TSVs) that are ~10 μm wide. The DRAM layers are separated from each other and from the base logic die by a 65 μm thick layer with polymer and solder bumps.

Figure 1 shows the 1.2 × 1.1 mm^2 cross section of the middle of HBM2 reconstructed via x-ray computed tomography. HBM2 has a 4 stacks of dynamic random access memory (DRAM) followed by a base layer of logic die [11]. Through silicon vias (TSV) are the primary carriers of current in the silicon layer, and the TSVs of different layers are connected via solder bumps [10], [11]. Polymer fillers separate different layers of silicon dies [12]. From the x-ray tomography, we measure that the top DRAM die is ~ 120 μm thick, while all the other DRAM layers are ~75 μm thick and the bottom logic die is ~ 150 μm thick. In the x-ray tomography image, we clearly

observe TSVs in the top DRAM layer and the logic die, while the TSVs appear smeared in middle DRAM layers. This observation is true for all the reconstructed cross sections of HBM. In our thermal analysis, however, we assume uniform thermal properties of all DRAM layers and the base die. Each polymer/solder bump layer is ~ 65 μm thick.

Since the boundaries of the layers are not clearly recognizable in the image, we estimate an uncertainty of ± 5 μm for each layer. This uncertainty in the thickness contributes to ~ 5% uncertainty in the thermal conductivity of the DRAM layers and ~ 7% uncertainty in the thermal conductivity of the polymer/solder bump layers.

2.3 Energy Dispersive X-ray Fluorescence (EDXRF)

We used energy dispersive x-ray fluorescence (EDXRF) spectroscopy to estimate the abundance of different metals in through silicon vias and solder bump layers in HBMs. The measurement was carried out in a Shimadzu EDXRF 7000 system with a Rh anode with a 50 keV peak energy used for the XRF excitation. We estimate the composition of through-silicon-vias from the intensities of the characteristic fluorescence x-rays using the fundamental parameters (FP) [13] methods using Shimadzu PCEDX Navi software.

The excitation x-ray was incident on the top DRAM layer, and the fluorescent x-rays escaping from the same front side were collected. Under the assumption that all the elements are distributed homogenously in the HBM, the FP method predicts an HBM to have 80% silicon, 10% copper, 3% tin, 2% nickel, 1.5% tungsten and 0.2% gold. However, different elements are present at different depths in the HBM. Fluorescent x-rays from elements present deeper inside the HBM undergo larger attenuation. Therefore, XRF cannot be used quantitatively.

We estimate the through-Si-vias (TSV) to be primarily copper with small amount of tungsten [14], [15]. From Ni K-alpha and Sn K-alpha we can estimate nickel and tin are present deeper inside the HBM as solder bump pads [16] and solder [17] respectively. Based on the trace amount of gold present, we predict the solder has gold along with tin. XRF also showed the presence of titanium (1%) and tantalum (1%) which are respectively used for adhesion [18] and prevention of electron migration [19].

3. DETERMINATION OF THERMAL CONDUCTIVITIES WITH 3ω

The 3ω method is a thermal conductivity measurement technique where a thin film metal heater prepared on the surface of a sample is Joule heated with an ac current with frequency ω. The I^2R heating of the sample, for an ac current amplitude I and the heater resistance R, causes temperature oscillations at 2ω on the heater, which can also be used as a resistance temperature detection (RTD) sensor for measuring the surface temperature. The 2ω oscillations in temperature results in 2ω oscillations of the resistance of the heater. The resulting voltage across the heater/sensor at 3ω measured using a lock-in amplifier measures the temperature oscillations of the sensor, which in turn, combined with the heat diffusion equation measures the thermal properties of the sample [6], [8].

3.1 Sample preparation for different heating geometries

We deposited two different shapes of 3ω heaters, i.e., a line/wire heater for cylindrical heating geometry, and a serpentine heater for a planar heating geometry, for making the measurement sensitive to different layers in an HBM. Silver heaters/sensors for 3ω were deposited through shadow masks using thermal evaporation. The shapes of the heaters used for planar and cylindrical heating geometry are shown in the schematic in Figure 2. For 3ω using a single wire heater, the

heater had a width of 250 µm, length of 5 mm, and a thickness of 100 nm. For planar heating, the serpentine heater had a total area of 5×9 mm^2 heater and a thickness of 70 nm. A 10 nm layer of chromium was deposited via the shadow masks for both the heater shapes to ensure the adhesion of silver to the sample.

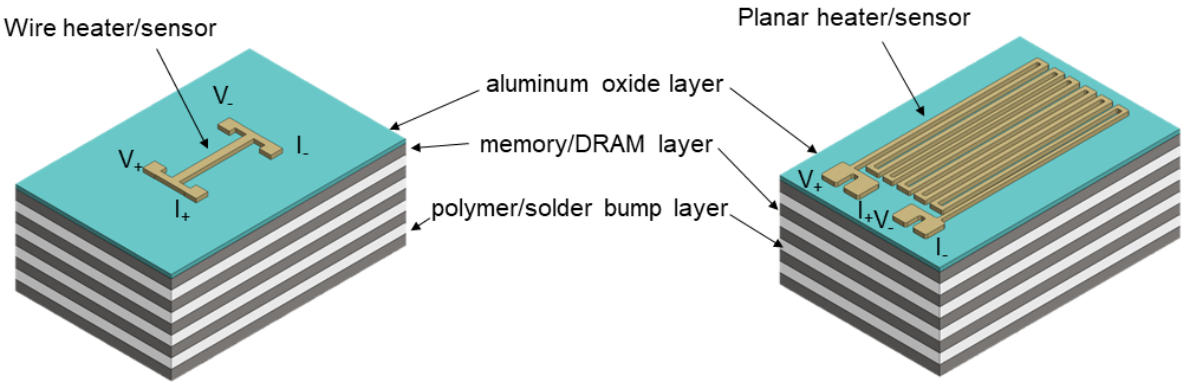

Figure 2. Schematic of the heater/sensor and layers used in the 3ω analysis. The alumina insulation is represented in teal while the DRAM and base die layers are represented in grey, and the polymer layers are represented in white. The sample with wire heater/sensor is shown in the left while the sample with the serpentine heater sensor (used for planar heat flow geometry) is shown in the right. The layers are not drawn to scale. The actual thickness of the alumina layer is 700 nm for the sample with the wire heater and 6 µm for the sample with the serpentine heater. The top DRAM layer is ~ 120 µm, the base logic die is ~150 µm and the other DRAM layers are ~ 80 µm. Each polymer layer is ~65 µm. The x-y dimension of HBM2 is 6×10 mm^2 on the top and 7×11 mm^2 on the bottom. The serpentine heater has an area of 5×9 mm^2.

To ensure the ac current was limited within the metallic heater used in 3ω, the top HBM die was insulated with a coating Al_2O_3 deposited via reactive DC magnetron sputtering of aluminum in an oxygen environment [20]. For 3ω using the wire heater, we deposited a thin layer of alumina to ensure sensitivity of the measurement to the first die in the HBM. From optical ellipsometry, we determine that the thickness of the alumina layer is ~ 700 nm. For planar heater geometry, since

the measurement is not sensitive to the top layer, we deposited a 6 μm alumina layer (estimated using crystal monitor) to ensure proper insulation.

We determined the room temperature 4-point resistance and the temperature coefficient of resistance of the 3ω heaters using Keithley 2000 digital multimeter. The 4-point resistances of the wire heater and planar heaters were 4.17 Ω and 214 Ω respectively. For the measurement of the temperature coefficient of resistance, the sample was mounted on a Peltier module attached to a heat sink. The temperature of the side attached to the sample was monitored using a K-type thermocouple, and the temperature was varied using a dc current source. 4-point resistance measurements were performed at 4 different temperature points at steps of ~10 ℃. The measurements were repeated 4 times. The temperature coefficient of resistance for the wire heater was $(2.4\pm0.1)\times10^{-3}$ $℃^{-1}$. The 4-point temperature coefficient of resistance of the serpentine heater was $(2.3\pm0.1)\times10^{-3}$ $℃^{-1}$. The 5% uncertainty in the RTD values induces uncertainty in the determined values of thermal conductivity. We estimate this uncertainty in the section on the sensitivity analysis.

The values of the temperature coefficient of resistance are lower compared to the value in bulk silver, i.e., 3.8×10^{-3} $℃^{-1}$. This is possibly due to significant grain boundary resistance in the polycrystalline silver films or the incorporation of oxygen impurities.

3.2. 3ω measurements

We use a SR830 lock-in amplifier to record the 3ω in-phase and out-of-phase voltages. The lock-in also acts as a voltage source to supply the ac current through the 3ω heaters. We use a cancellation circuit similar to one described by Cahill [6] using a 10-turn variable resistors resistor in series with the 3ω heater to suppress the 1ω voltage in the lock-in amplifier. The voltage drops

across the variable resistor and the 3ω heater are isolated using a pair of AD524 instrumentation amplifiers. The potential difference across the 3ω heater is fed to channel A of the SR830 lock-in and the potential difference across the variable resistor is fed to channel B. The lock-in is then operated to record the differential voltage, and the 10-turn resistor is varied until the differential 1ω voltage reduces to an acceptable value. The measurements are then carried out in the third harmonic to record the 3ω in-phase and out-of-phase voltage.

The 1ω voltage drop across the sample, recorded by channel A of the lock-in amplifier, divided by the resistance of the heater determined from the 4-point resistance measurement, provides the current across the sample. In our measurement, we could obtain 70 mA current across the wire heater and 10 mA current across the serpentine heater using the maximum output voltage of SR830, i.e., 5V.

3.3 Sensitivity analysis for cylindrical and planar heating geometries

For a planar heat flow geometry, Feldman provided the analytical solution to the temperature response in any arbitrary layer due to a modulated heating in any layer [21]. Feldman later extended his algorithm to the temperature response in a line heater due to cylindrical heating [22].

We use the Feldman algorithms for cylindrical and planar heating along with sensitivity analysis to determine which thermal properties can be determined from in-phase and out-of-phase temperature oscillations during 3ω measurements.

The sensitivity coefficient ξ_p^S, defined as $\xi_p^S = \frac{d \ln S}{d \ln p}$ for a parameter p and signal S, measures the percentage change in the signal S for 1% change in a parameter p [7].

The modelling of the layers used for the sensitivity analysis and fitting the experimental data resembles the schematic shown in Figure 2 (the figure is not drawn to scale). The model contains 5 memory layers (i.e., 4 DRAM layers and a base die) with the thickness of the top and bottom layers as 120 µm and 150 µm respectively. The thickness of the other three DRAM layers is 80 µm each. The layers are separated by polymer/solder bump layers, each 65 µm thick.

3ω measurements are performed by sandwiching the sample in between two pieces of a coarse polymer foam (a common kitchen sponge) to prevent convective losses. The density of the sponge is ~ 0.1 g/cm^3, and therefore we set the heat capacity and thermal conductivity of the sponge to 0.05 W/m-K and 100 kJ/m^3 for our thermal analysis. The measurement does not have a significant sensitivity to these values if convective losses are suppressed.

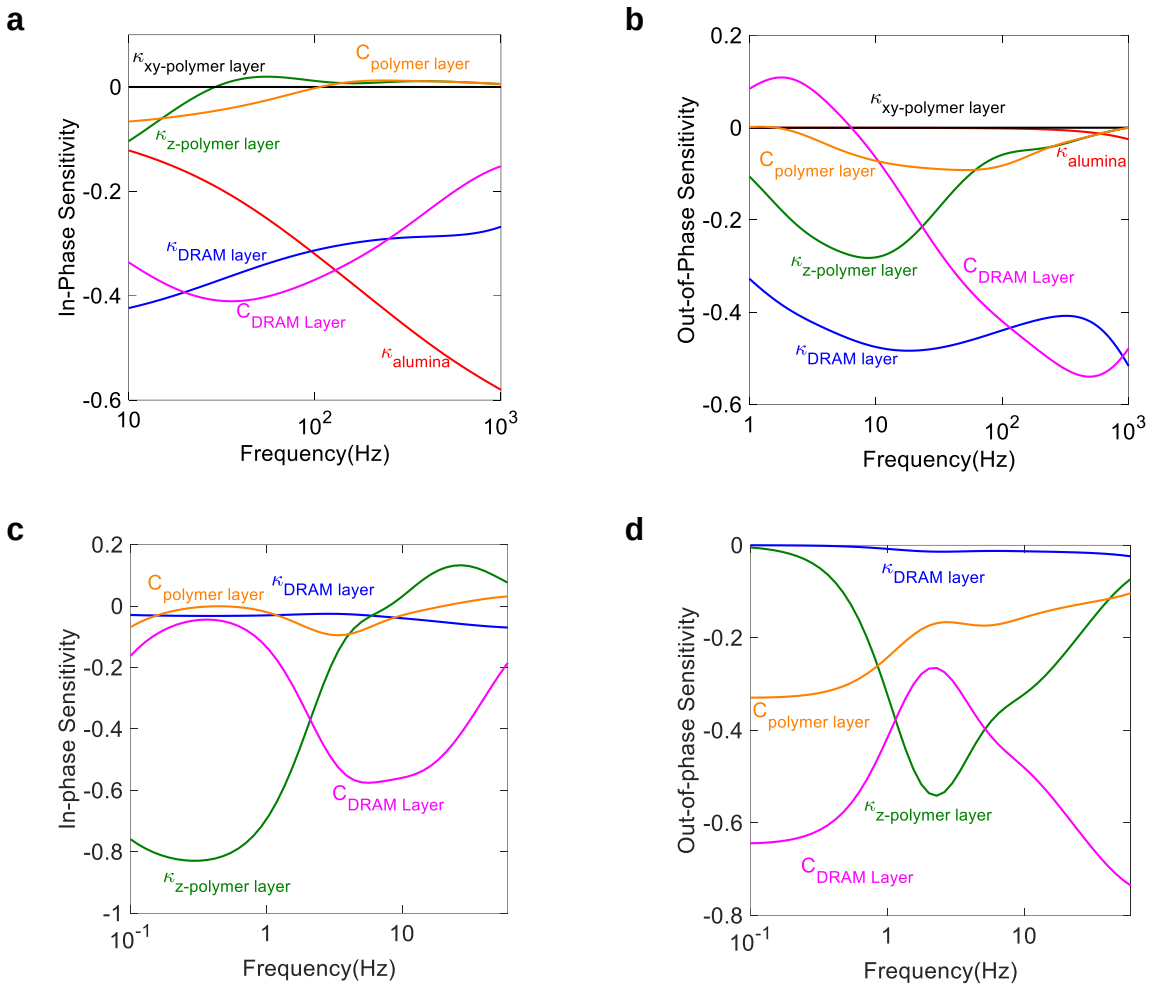

Figure 3. Sensitivity of thermal conductivity and volumetric heat capacity for different layers in the 3ω measurement of HBM. (a) and (b) show the sensitivities for the respective in-phase and out-of-phase temperature oscillations for the 3ω measurement with a wire heater/sensor. (c) and (d) show the sensitivities for the respective in-phase and out-of-phase temperature oscillations for the 3ω measurement with a planar heater/sensor. The sensitivities to the thermal conductivities of the aluminum oxide insulation layer, the DRAM/memory layer and the in-plane and through-plane thermal conductivities of the polymer layer are represented by red, blue, green and black solid lines respectively. The sensitivity to the aluminum oxide layer is not shown for (c) and (d) as the sensitivity is small, comparable to the sensitivity to the DRAM layer across the frequency range of the measurement. The sensitivities to the volumetric heat capacity of the memory and polymer layers are represented by magenta and orange solid lines respectively. The sensitivity calculation is performed on an HBM sample sandwiched between sponge with thermal conductivity of 0.05 W/m-K and a volumetric heat capacity of 0.1 MJ/K. The values of the thermal conductivity of the alumina layer, the memory layer, the polymer/solder bump layer along z-direction and the polymer/solder bump layer along xy-direction used for the analysis are 1.7 W/m-K, 140 W/m-K, 2 W/m-K and 0.1 W/m-K. The volumetric heat capacities of the alumina, memory and polymer are 3.1 W/m-K, 2.6 W/m-K and 2.6 W/m-K respectively.

For the wire heater, the temperature response on the surface is primarily determined by the highly conductive top DRAM layer, which spreads the heat in the in-plane direction. This can be seen in Figures 3a and 3b, where the parameters most sensitive to the measurement are thermal conductivity and the specific heat capacity of the top DRAM layer. The in-phase temperature response, when using the wire heater, also depends on the thermal conductivity of the aluminum oxide layer used for insulation. The value of thermal conductivity of aluminum oxide, 1.7 W/m-K, has been measured in the past for reactively sputtered aluminum oxide [23]. Therefore, the thermal conductivity of the top DRAM layer can be estimated accurately from the 3ω measurement using the wire heater, once the specific heat capacity is estimated. Since the sensitivity of the measurement to the thermal conductivity of the top DRAM layer is ~ 0.5 for the entire range of frequency, we estimate that a 4% uncertainty in the RTD calibration results in an 8% uncertainty in the thermal conductivity of the top DRAM layer.

At lower frequencies, the 3ω measurement using a wire heater/sensor is slightly sensitive to the through-plane conductivity of the polymer/layer. The measurement is not sensitive to the in-plane thermal conductivity of the polymer layer due to the presence of low conductivity polymers which do not contribute to the heat transfer significantly. In our measurement and analysis, we estimate the in-plane conductivity of the polymer layer to be equal to a typical polymer, i.e., 0.1 W/m-K.

We restrict our 3ω measurement using the wire heater from 10 Hz to 1000 Hz. At 10 Hz, the expected thermal penetration depth in the in-plane direction of the topmost DRAM layer is ~ 2 mm, which is smaller than the width of the sample (6 mm). Below 10 Hz, the finite lateral dimension of the sample contradicts the assumption of infinitely large x-y dimension of the sample used in analytical modelling. Above 1000 Hz, the 3ω signal is too small.

For the 3ω measurement using the planar heater, we perform the measurements from 0.1 Hz to 60 Hz. Above 60 Hz, the 3ω signal was too small due to the small current that could be applied. Below 0.1 Hz, the measurement time would be very long, without providing additional information on the thermal properties of the sample.

Figure 3c and 3d show the in-phase and out-of-phase temperature oscillations using the planar heater. The heater dimension used in the analysis is 6×10 mm^2 as the thermal penetration depth of the ~ 0.5 mm or larger in the lateral dimension for the entire range of frequency used in our measurement. Therefore, the heat flow is restricted to the through plane direction.

The out-of-phase temperature oscillation at low frequency is primarily determined by the heat capacity of the sample. Therefore, we can use the out-of-phase 3ω measurement using planar heating to estimate the effective heat capacity of the sample. The measurement cannot distinguish between the heat capacities of the polymer and the memory layers. Therefore, we use a single value of heat capacity to fit the polymer and memory layers and the logic die.

In the planar heat flow geometry, the in-phase temperature response at the measurement frequencies of 0.1 Hz to 60 Hz is primarily determined by the thermal conductivity of the polymer layer which has a high thermal resistance compared to the DRAM layer. The sensitivity of the in-phase temperature oscillations to the through-plane conductivity of the polymer layer is ~ 0.8 at frequencies below 1 Hz. Therefore, the 4% uncertainty in the RTD calibration only contributes to ~ 5 % uncertainty in the best-fit value of thermal conductivity of the polymer layer determined with planar heating.

3.4 Results

The best-fit to the experimental 3ω data utilizing wire and planar heaters/sensors are shown in Figure 4a and 4b respectively.

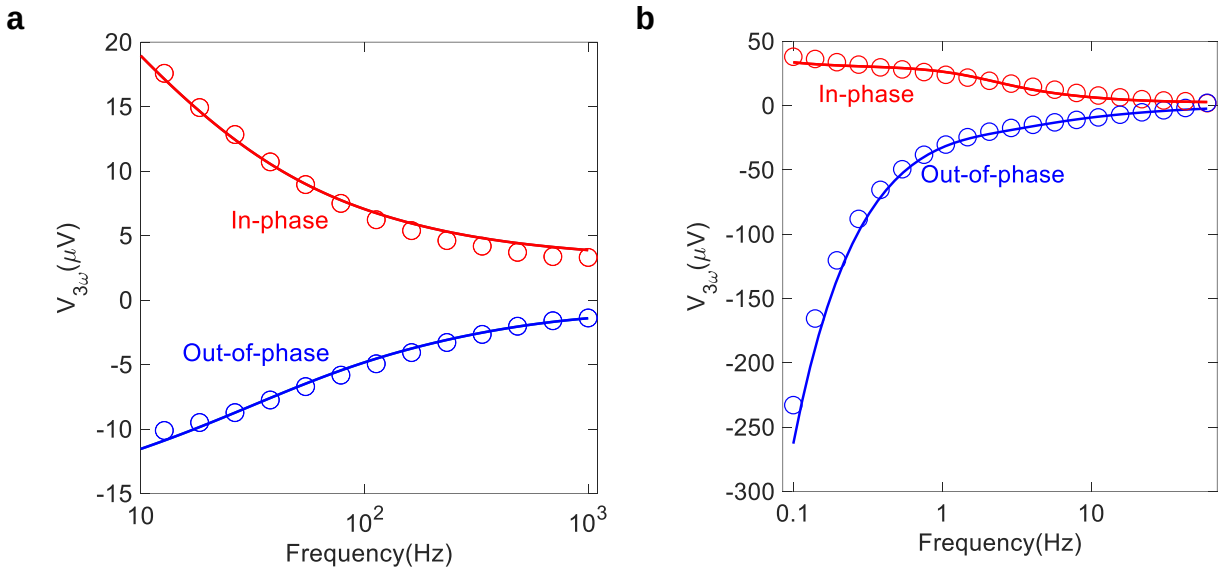

Figure 4. Experimental 3ω data (open circles) and the best fit (solid lines) for (a) wire heater/sensor and (b) planar heater/sensor. The in-phase values are represented in red while the out-of-phase values are represented by blue.

Using the best-fit to the experimental data for the out-of-phase voltage for the 3ω measurements using the planar heater, we determine the heat capacity of the memory and DRAM layers to be 2.6 W/m-K. This is about 30% higher than what we expect from a sample primarily containing silicon, polymer and tin and a small amount of copper.

From the best-fit to the in-phase 3ω voltage for the planar heating, we estimate the through-plane thermal conductivity of the polymer/solder bump layer is 2 W/m-K. Taking into account the uncertainties in the measurement induced due to the uncertainty in the thickness (7%) and the uncertainty in RTD calibration (5%), we estimate a total uncertainty of 9%. Therefore, the through-thickness thermal conductivity of the polymer layer is 2 ± 0.2 W/m-K.

This value of the through-plane conductivity of the polymer/solder bump layer is surprisingly low, given that x-ray tomography shows, approximately 20% of the layer is occupied by tin solder bumps. Previous studies have reported that the values of the thermal conductivity of tin alloys used for soldering are typically around 60 W/m-K [24], [25], while the thermal conductivity of bulk tin is about 65 W/m-K [26]. Therefore, we would expect the through-plane thermal conductivity of the polymer/solder bump layer to near 10 W/m-K.

Finally, using the best fit to the in-phase and out-of-phase data for the 3ω measurements with the wire heater, we measure the in-plane thermal conductivity of the memory layer to be 140 W/m-K. With the uncertainties in the measurement resulting from uncertainties in thickness (5 %) and RTD calibration (8%), the thermal conductivity of the memory layer is 140 ± 13 W/m-K. This value is expected for a layer that is predominantly silicon.

Combining the results of the thermal conductivity measurements with the results from x-ray tomography, we can estimate the effective in-plane and through-plane thermal conductivity of the overall HBM device. Using a parallel resistance model for thermal resistance, the effective in-plane conductivity of the HBM is 100 ±10 W/m-K while using the series resistance model for thermal resistance, the effective through plane conductivity is 7 ± 0.7 W/m-K.

4. DISCUSSION AND CONCLUSIONS

With the combination of different heating geometries using 3ω and x-ray computed tomography, we determined the in-plane and through plane thermal conductivity of HBM. A similar approach can be generally used to determine the thermal conductivity of individual layers and the effective thermal conductivities in 3D ICs.

With regards to the present work, the measured in-plane conductivity of the top layer of ~ 140 W/m-K is expected [27] as the sample is mostly silicon with a small volume of deposited copper in the form of through-Si-vias. However, the expected through plane conductivity is quite low assuming ~ 20% of the polymer area is comprised by solder bumps. This indicates either that the metals deposited in the manufacturing process have significantly smaller thermal conductivities compared to the previously reported values in tin alloys or the contact area of the solder bump to the silicon/TSV layer is small. This potentially has implications for the electrical performance of the device in addition to the thermal performance. Therefore, effective thermal management of 3D ICs requires focusing on the manufacturing processes where the thermal conductivities of the deposited metals are not significantly reduced from their bulk values and ensuring a possibly larger contact between solder bumps and TSVs.

ACKNOWLEDGEMENTS

The authors thank Dr. Tanya Josek of the Beckman Microscopy Suite, University of Illinois for assistance with the X-ray tomography measurements and Zingyi Zhou of the Department of Materials Science, University of Illinois for help with ellipsometry. Part of this work was carried out at the Materials Research Laboratory at the University of Illinois. This work was supported by Semiconductor Research Corporation (Task ID: 3044.001).

References

[1] D. Chalise, P. Kenesei, S. D. Shastri, and D. G. Cahill, “Temperature mapping of stacked silicon dies using x-ray diffraction intensities,” *Phys. Rev. Appl.*, 2022.

[2] H. F. Hamann *et al.*, “Hotspot-limited microprocessors: Direct temperature and power distribution measurements,” *IEEE J. Solid-State Circuits*, vol. 42, no. 1, pp. 56–64, 2007,

doi: 10.1109/JSSC.2006.885064.

[3] H. Prajapati, D. Chalise, D. Ravoori, R. M. Taylor, and A. Jain, “Improvement in build-direction thermal conductivity in extrusion-based polymer additive manufacturing through thermal annealing,” *Addit. Manuf.*, vol. 26, no. October 2018, pp. 242–249, 2019, doi: 10.1016/j.addma.2019.01.004.

[4] C. Monachon, L. Weber, and C. Dames, “Thermal Boundary Conductance: A Materials Science Perspective,” *Annu. Rev. Mater. Res.*, vol. 46, pp. 433–463, 2016, doi: 10.1146/annurev-matsci-070115-031719.

[5] D. G. Cahill, “Analysis of heat flow in layered structures for time-domain thermoreflectance,” *Rev. Sci. Instrum.*, vol. 75, no. 12, pp. 5119–5122, 2004, doi: 10.1063/1.1819431.

[6] D. G. Cahill, “Thermal conductivity measurement from 30 to 750 K: The 3ω method,” *Rev. Sci. Instrum.*, vol. 61, no. 2, pp. 802–808, 1990, doi: 10.1063/1.1141498.

[7] P. Jiang, X. Qian, and R. Yang, “Time-domain thermoreflectance (TDTR) measurements of anisotropic thermal conductivity using a variable spot size approach,” *Rev. Sci. Instrum.*, vol. 88, no. 7, 2017, doi: 10.1063/1.4991715.

[8] C. Dames, “Measuring the Thermal Conductivity of Thin Films: 3 Omega and Related Electrothermal Methods,” *Annu. Rev. Heat Transf.*, vol. 16, no. 1, pp. 7–49, 2013, doi: 10.1615/annualrevheattransfer.v16.20.

[9] S. D. Lubner, S. Kaur, Y. Fu, V. Battaglia, and R. S. Prasher, “Identification and characterization of the dominant thermal resistance in lithium-ion batteries using operando

3-omega sensors," *J. Appl. Phys.*, vol. 127, no. 10, 2020, doi: 10.1063/1.5134459.

[10] S. Kim *et al.*, "Signal Integrity Design and Analysis of a Spiral Through-Silicon Via (TSV) Array Channel for High Bandwidth Memory (HBM)," *IEEE Electr. Des. Adv. Packag. Syst. Symp.*, vol. 2021-Decem, no. Il, pp. 2021–2023, 2021, doi: 10.1109/EDAPS53774.2021.9657033.

[11] K. Kim *et al.*, "Deep Reinforcement Learning-based through Silicon Via (TSV) Array Design Optimization Method considering Crosstalk," *IEEE Electr. Des. Adv. Packag. Syst. Symp.*, vol. 2020-Decem, pp. 1–3, 2020, doi: 10.1109/EDAPS50281.2020.9312906.

[12] S. Md Zulkifli, B. Zee, W. Qiu, and A. Gu, "High-Res 3D X-ray microscopy for non-destructive failure analysis of chip-to-chip micro-bump interconnects in stacked die packages," *Proc. Int. Symp. Phys. Fail. Anal. Integr. Circuits, IPFA*, vol. 2017-July, pp. 1–5, 2017, doi: 10.1109/IPFA.2017.8060111.

[13] J. W. Criss and L. S. Birks, "Calculation Methods for Fluorescent X-Ray Spectrometry: Empirical Coefficients vs. Fundamental Parameters," *Anal. Chem.*, vol. 40, no. 7, pp. 1080–1086, 1968, doi: 10.1021/ac60263a023.

[14] K. Kondo *et al.*, "High-Aspect-Ratio Copper-Via-Filling for Three-Dimensional Chip Stacking," *J. Electrochem. Soc.*, vol. 152, no. 11, p. H173, 2005, doi: 10.1149/1.2041047.

[15] B. Horváth, J. Kawakita, and T. Chikyow, "Through silicon via filling methods with metal/polymer composite for three-dimensional LSI," *Jpn. J. Appl. Phys.*, vol. 53, no. 6 SPEC. ISSUE, 2014, doi: 10.7567/JJAP.53.06JH01.

[16] K. Y. Au *et al.*, "Multi Chip Stacking & Reliability Challenges using TSV - Micro C4

Solder Interconnection for FCCSP TSV package," pp. 608–619, 2011.

[17] R. Agarwal *et al.*, "Cu / Sn Microbumps Interconnect for 3D TSV Chip Stacking," no. i, pp. 858–863, 2010.

[18] S. J. Hong, S. C. Hong, W. J. Kim, and J. P. Jung, "Copper Filling to TSV (Through-Si-Via) and Simplification of Bumping Process," *J. Microelectron. Packag. Soc.*, vol. 17, no. 3, pp. 79–84, 2010.

[19] V. Brize *et al.*, "ALD TaN from PDMAT in TSV architecutres," *ECS Trans.*, vol. 33, no. 2, pp. 183–193, 2010.

[20] W. D. Sproul, M. E. Graham, M. S. Wong, S. Lopez, D. Li, and R. A. Scholl, "Reactive direct current magnetron sputtering of aluminum oxide coatings," *J. Vac. Sci. Technol. A Vacuum, Surfaces, Film.*, vol. 13, no. 3, pp. 1188–1191, 1995, doi: 10.1116/1.579859.

[21] A. Feldman, "Algorithm for solutions of the thermal diffusion equation in a stratified medium with a modulated heating source," *High Temp. - High Press.*, vol. 31, no. 3, pp. 293–296, 1999, doi: 10.1068/htrt171.

[22] J. H. Kim, A. Feldman, and D. Novotny, "Application of the three omega thermal conductivity measurement method to a film on a substrate of finite thickness," *J. Appl. Phys.*, vol. 86, no. 7, pp. 3959–3963, 1999, doi: 10.1063/1.371314.

[23] S. M. Lee and D. G. Cahill, "Thermal conductivity of sputtered oxide films," *Phys. Rev. B*, vol. 52, no. 1, pp. 253–257, 1995, doi: 10.1016/b978-0-408-01190-7.50016-9.

[24] D. Suraski and K. Seelig, "The current status of lead-free solder alloys," *IEEE Trans. Electron. Packag. Manuf.*, vol. 24, no. 4, pp. 244–248, 2001, doi: 10.1109/6104.980031.

[25] J. Bilek, J. Atkinson, and W. Wakeham, “Thermal Conductivity of Molten Lead Free Solders,” in *Europeam Microlectronics and Packaging Symposium*, 2004, no. June.

[26] E. Yamasue, M. Susa, H. Fukuyama, and K. Nagata, “Deviation from Wiedemann – Franz Law for the at Elevated Temperature 1,” *Int. J.*, vol. 24, no. 3, pp. 2–12, 2003.

[27] M. G. Burzo, P. L. Komarov, and P. E. Raad, “Non-contact thermal conductivity measurements of P-doped and N-doped gold covered natural and isotopically-pure silicon and their oxides,” *Proc. 5th Int. Conf. Therm. Mech. Simul. Exp. Microelectron. Microsystems, EuroSimE 2004*, pp. 269–276, 2004, doi: 10.1109/esime.2004.1304050.